Porous Metal-Organic Framework CUK-1 for Adsorption Heat Allocation toward Green Applications of Natural Refrigerant Water

Lee, Ji Sun; Yoon, Ji Woong; Mileo, Paulo G.M.; Cho, Kyung Ho; Park, Jaedeuk; Kim, Kiwoong; Kim, Hyungjun; de Lange, Martijn F.; Kapteijn, Freek; More Authors

DOI
10.1021/acsami.9b02605

Publication date
2019

Document Version
Final published version

Published in
ACS applied materials & interfaces

Citation (APA)
Lee, J. S., Yoon, J. W., Mileo, P. G. M., Cho, K. H., Park, J., Kim, K., Kim, H., de Lange, M. F., Kapteijn, F., & More Authors (2019). Porous Metal-Organic Framework CUK-1 for Adsorption Heat Allocation toward Green Applications of Natural Refrigerant Water. *ACS applied materials & interfaces*, *11*(29), 25778-25789. https://doi.org/10.1021/acsami.9b02605

ACS APPLIED MATERIALS & INTERFACES

Research Article

Cite This: ACS Appl. Mater. Interfaces 2019, 11, 25778−25789

www.acsami.org

Porous Metal−Organic Framework CUK-1 for Adsorption Heat Allocation toward Green Applications of Natural Refrigerant Water

Ji Sun Lee,[†] Ji Woong Yoon,[†] Paulo G. M. Mileo,[‡] Kyung Ho Cho,[†] Jaedeuk Park,[†] Kiwoong Kim,[†] Hyungjun Kim,[§] Martijn F. de Lange,[∥] Freek Kapteijn,[∥] Guillaume Maurin,*[,‡] Simon M. Humphrey,*[,⊥] and Jong-San Chang*[,†,#]

[†]Research Group for Nanocatalyst and Chemical Safety Research Center, Korea Research Institute of Chemical Technology (KRICT), Gajeong-ro 141, Yuseong-gu, Daejeon 34114, South Korea

[‡]Institut Charles Gerhardt, Montepellier, UMR 5253 CNRS ENSCM UM, Université Montpellier, Montpellier Cedex 05 34095, France

[§]Graduate School of Energy, Environment, Water and Sustainability, Korea Advanced Institute of Science and Technology (KAIST), Daehak-ro 291, Yuseong-gu, Daejeon 34141, South Korea

[∥]Catalysis Engineering−Chemical Engineering Department, Delft University of Technology, Van der Maasweg 9, Delft 2629 HZ, The Netherlands

[⊥]Department of Chemistry, The University of Texas at Austin, 2.204 Welch Hall, 105 E. 24th St. Stop A5300, Austin, Texas 78712, United States

[#]Department of Chemistry, Sungkyunkwan University, Suwon 440-476, South Korea

Supporting Information

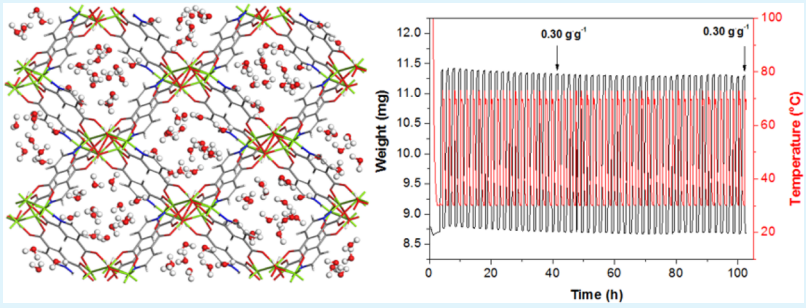

ABSTRACT: The development of new water adsorbents that are hydrothermally stable and can operate more efficiently than existing materials is essential for the advancement of water adsorption-driven chillers. Most of the existing benchmark materials and related systems in this field suffer from clear limitations that must be overcome to meet global requirements for sustainable and green energy production and utilization. Here, we report the energy-efficient water sorption properties of three isostructural metal−organic frameworks (MOFs) based on the simple ligand pyridine-2,4-dicarboxylate, named M-CUK-1 [$M_3(\mu_3\text{-}OH)_2(2,4\text{-}pdc)_2$] (where M = Co^{2+}, Ni^{2+}, or Mg^{2+}). The highly hydrothermally stable CUK-1 series feature step-like water adsorption isotherms, relatively high H_2O sorption capacities between P/P_0 = 0.10−0.25, stable cycling, facile regeneration, and, most importantly, benchmark coefficient of performance values for cooling and heating at a low driving temperature. Furthermore, these MOFs are prepared under green hydrothermal conditions in aqueous solutions. Our joint experimental−computational approach revealed that M-CUK-1 integrates several optimal features, resulting in promising materials as advanced water adsorbents for adsorption-driven cooling and heating applications.

KEYWORDS: *metal−organic framework, water sorption, M-CUK-1, coefficient of performance, SAPO-34*

1. INTRODUCTION

Recent advances in sustainable and green chemistry have focused on global issues such as climate change, energy production, availability of a safe and adequate water supply, and the use of water as a clean reaction/synthesis medium.[1,2] Water is one of the oldest refrigerants and an environmentally friendly natural refrigerant that has attracted renewed interest because it is inherently benign, nonflammable, abundant, and essentially cost-free.[3] Therefore, the implementation of water as a refrigerant has been intensively considered in recent years for applications traditionally served by fluorocarbons.[4] Global energy consumption for heating and cooling in residential

Received: February 14, 2019
Accepted: July 1, 2019
Published: July 1, 2019

DOI: 10.1021/acsami.9b02605
ACS Appl. Mater. Interfaces 2019, 11, 25778−25789

areas has increased steadily over the past few decades and it is forecasted to accelerate in the coming years, especially for cooling purposes.[5] However, the current infrastructure relies primarily on nonsustainable energy resources; this is in misalignment with recent global agreements that aim to reduce our dependence on energy generation from fossil fuels.[6,7]

When water evaporates under vacuum, it is cooled because of the substantial latent heat of evaporation (2500 kJ kg^{-1} or 40.7 kJ mol^{-1}). By exploiting this phenomenon, water has been touted as a "natural" refrigerant fluid for adsorption-driven chiller/heat pump applications.[8−13] The adsorption-driven chiller/heat pump technology features a two-step process comprising a working cycle and a regeneration cycle. The regeneration cycle of the adsorbent after the working cycle requires external work in the form of thermal energy input.

Ideally, the regeneration temperature should be as low as possible (below 80 °C) to enable the use of low-grade and environmentally sensitive heat sources (e.g., industrial waste heat or solar energy). Such an arrangement could be considered to be a sustainable and more energy-efficient solution for both heating and cooling requirements.[8] The implementation of this plan depends, in part, on the development of new materials that can act as green water adsorbents. Water adsorbents play a crucial role in ensuring energy-efficiency of adsorption chillers and heat pumps.[8] Additionally, thermal energy storage by the so-called "thermal batteries", based on reversible adsorption/desorption of water as a working fluid rather than by conventional vapor compression, is a promising alternative to exploit waste thermal energy for heat re-allocation.[8] A suitable water adsorbent needs to fulfil the following five criteria under specific working conditions: have (i) a high working capacity on a volumetric (or gravimetric) basis; have (ii) high coefficient of performance (COP) values for cooling and heating, which indicate thermal energy efficiency; allow (iii) fast adsorption and desorption of water; permit (iv) regeneration at low temperature (<80 °C); and have (v) sufficient chemical and mechanical robustness, particularly being resistant to degradation in hot water vapor (i.e., steam).[14,15] In addition to these criteria, the synthesis cost of the selected adsorbent is an important economical consideration for large-scale implementation.

Silica gel and aluminosilicate zeolites are currently the standard materials employed as water adsorbents. Although these materials are relatively cheap and easy to prepare in large quantities, they suffer from distinct drawbacks for adsorption-chiller/heat pump applications, including weak hydrophilicity leading to water adsorption at rather high relative pressures (e.g., silica gel), and very strong hydrophilic character that necessitates the need for high regeneration temperatures (often >150 °C; e.g., aluminosilicate zeolites).[16] As an alternative, the CHA-type silico-aluminophosphate material SAPO-34 has emerged as a commercially viable adsorbent for adsorption-driven chillers because of its high water uptake at low relative pressure, combined with its very high durability and robustness.[17,18] However, efforts to develop more advanced water adsorbents are both critical and timely as the working capacities of these commercial adsorbents at low pressure (P/P_0 = 0.15−0.35) are not large enough.

Metal−organic frameworks (MOFs) are a contemporary class of microporous materials that are characterized by having broadly tunable structural and chemical properties, owing to an essentially unlimited combination of inorganic metal and organic linker components available for their synthesis.[19−21] In the context of the water adsorption-driven chiller/heat pump applications, the richness of this family of materials leverages the ability to modulate the hydrophilic/hydrophobic environment of the micropores via synthetic design to an extent that is not possible for classical aluminosilicate materials. This can be achieved by incorporating particular functional groups within the MOF framework. In 2006, Chang and co-workers were the first to report an energy-efficient sorption of water by MOF adsorbents, exhibiting large water uptakes and easy regeneration at low temperature, that is below 80 °C.[22] Specifically, we reported the energy-efficient dehumidification by the hydrothermally stable mesoporous metal(III) polycarboxylate MOFs, MIL-100 and MIL-101, which showed exceptional water sorption loading capacities and low associated regeneration energy penalties.[23] Subsequently, Henninger and Janiak proposed a heat transformation application using the MOF ISE-1 as a water adsorbent.[24] Since these pioneering reports, several more MOFs have been reported as promising candidates for water sorption applications.[8,9,25−30] However, none of the MOFs studied so far have completely fulfilled all five criteria mentioned above, required for adsorption chiller and/or heat pump applications. Here, we propose M-CUK-1 (CUK = Cambridge-University-KRICT), comprising metal(II) cations and the dianion of pyridine-2,4-dicarboxylic acid (2,4-$pdcH_2$)[31] as viable candidates for cooling and heating at low driving temperatures, owing to their remarkable coefficients of performance under realistic working conditions, combined with their very high hydrothermal stability and ease of regeneration. The M-CUK-1 materials can also be easily tuned in terms of chemical modulation of the inorganic structural components, that is, by obtaining isostructural materials based on 3s- or 3d-metals, Mg^{2+}, Co^{2+}, or Ni^{2+}.[32,33] This assertion is demonstrated and confirmed by a combined experimental and computational investigation that integrates gravimetric sorption testing, thermodynamic calculations of cooling/heating performances, and molecular simulations. This work equally aims to investigate the energy-efficient water sorption properties of M-CUK-1 materials that could be potentially applied to thermal energy storage as well as for adsorption-driven heating/cooling.

2. RESULTS AND DISCUSSION

2.1. Synthesis and Characterization of M-CUK-1 (M = Mg, Co, Ni). The Co(II)-based CUK-1 was the first phase reported in 2005;[34] this material was obtained by the hydrothermal reaction of pyridine-2,4-dicarboxylic acid (2,4-$pdcH_2$) and $CoCl_2$ with excess KOH in water at 200 °C for 15 h.[31] In the reaction, subcritical water under autogenous pressure provides a highly solubilizing reaction medium, and the forcing reaction conditions yield porous Co-CUK-1, $[Co_3(\mu_3\text{-}OH)_2(2,4\text{-}pdc)_2]\cdot 9H_2O$ as a single, crystalline phase. Co-CUK-1 cannot be obtained by conventional solvothermal synthesis.

As illustrated in Figure 1a, Co-CUK-1 has an infinite 1-dimensional microchannel system supported by highly connected 2,4-pdc ligands that are arranged in orthogonal fashion around edge- and vertex-sharing $M_3(OH)_2$ chains. The structural details of the CUK-1 materials are discussed in the previous papers.[31−33] The channels are filled with water molecules that can be fully removed by heating and/or under vacuum, without loss of crystallinity, as originally determined

DOI: 10.1021/acsami.9b02605
ACS Appl. Mater. Interfaces 2019, 11, 25778−25789

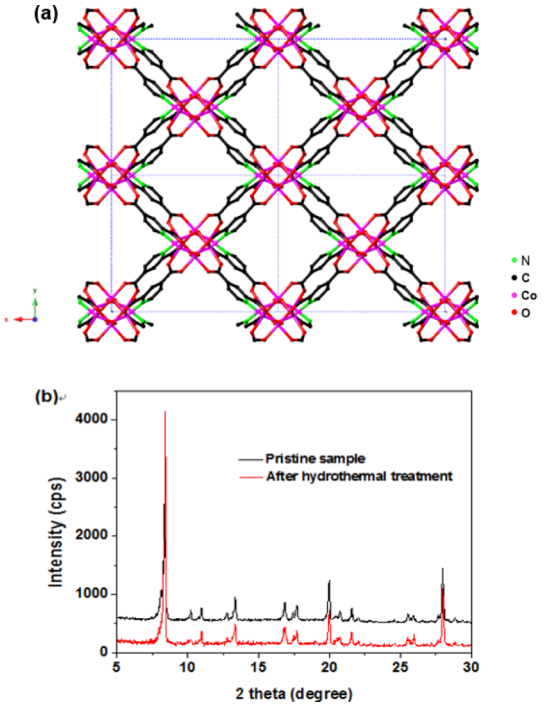

Figure 1. (a) Extended structure of desolvated Co-CUK-1 obtained by heating a single crystal to 100 °C in order to remove H_2O; the structural image of (a) shows the space-filling model and guest-accessible voids when viewed perpendicular to the direction of propagation of infinite 1-dimensional diamondoid channels. (b) PXRD patterns of Co-CUK-1 before and after hydrothermal treatment at 150 °C for 3 days.

by single-crystal X-ray diffraction (SCXRD) and bulk powder X-ray diffraction (PXRD) studies.[31]

Somewhat more recently, upon experimentation with other M(II) salts, two further analogues, Ni-CUK-1[32] and Mg-CUK-1,[33] were also identified using $NiCl_2$ in a 3:2:9 molar ratio of $NiCl_2$/2,4-pdcH_2/KOH, or $Mg(NO_3)_2$ in a 3:2:8 molar ratio of $Mg(NO_3)_2$/2,4-pdcH_2/KOH, respectively, by analogous hydrothermal heating methods between 200 and 220 °C. Both Ni and Mg materials are isostructural with the Co phase and the lattice connectivity is identical for the three frameworks. The space group of the as-synthesized Mg-CUK-1 was found to be of lower symmetry ($P2_1/c$ for the Mg-analogue vs $C2/c$ for the Co- and Ni-analogues) because of the positions of water molecules inside the pores; however, Mg-CUK-1 reverts to a *C*-centered cell setting upon desolvation.[33] The PXRD patterns of the three as-synthesized CUK-1 materials prepared in this work are actually concurrent with the simulated patterns obtained from the SCXRD structures.[31] Thermogravimetric analysis (TGA) profiles of the freshly prepared (hydrated) Co-CUK-1 and Ni-CUK-1 in a nitrogen carrier flow show close correlation in terms of their temperature-dependent mass loss behavior (Supporting Information Figure S1). There is a rapid loss of guest water molecules between 25 and 100 °C, which conforms very closely to the mass loss that is expected for $9H_2O$ per 3 M(II) ions (M = Co, Ni; observed mass loss = 22.4%; calculated = 21%) at which point the materials become resistant to any further mass loss because of a ligand-based decarboxylation until ca. 410 °C (Co-CUK-1) or 430 °C (Ni-CUK-1). The TGA for the hydrated Mg-CUK-1 confirmed a rapid 25% mass loss between 25 and 100 °C, after which there is a very large temperature window where Mg-CUK-1 remains thermally stable, until the onset of degradation at ca. 510 °C.

The larger initial weight loss of Mg-CUK-1 compared to the two other CUK-1 is due to the significantly lower mass of Mg^{2+} (i.e., Mg-CUK-1 is significantly less dense than the Co and Ni phases). Meanwhile, the higher thermal stability is attributed to the greater extent of electrostatic bonding between Mg^{2+} and the carboxylate-O donors. Overall, the TGA results evidenced that all M-CUK-1 are highly thermally robust, the Mg-version being more stable than the two 3d-metal analogues. CO_2 adsorption at −78.5 °C is commonly studied in the MOF literature, especially when cryogenic N_2 adsorption (at −196 °C) yields no information because of several possible limitations in terms of accessibility of the pores (case of ultrasmall pore MOFs) or/and very slow kinetics of the adsorbates (case of strongly hindered environment of the porosity). Typically, CO_2 physisorption at −78.5 °C was used to estimate the Brunauer−Emmett−Teller (BET) area of the Ca-based MOF UTSA-280, which does not adsorb N_2 at −196 °C.[35] For M-CUK-1, the adsorption isotherms of CO_2 at −78.5 °C were used to evaluate the BET areas (Figure S2) as the N_2 physisorption isotherm of Co-CUK-1 at −196 °C was not correctly obtained because of the low temperature phase transformation of this solid.[36,37] Fitting the BET equation to the resulting isotherms of CO_2 gives the following estimated BET areas: 510 $m^2\ g^{-1}$ (Co-CUK-1); 520 $m^2\ g^{-1}$ (Ni-CUK-1); 580 $m^2\ g^{-1}$ (Mg-CUK-1). The micropore volumes of M-CUK-1 were obtained from the CO_2 adsorption at −78.5 °C, by applying the Dubinin−Radushkevich equation.[38] The micropore volumes of all three analogues are similar: 0.26 mL g^{-1} (Co-CUK-1); 0.26 mL g^{-1} (Ni-CUK-1); and 0.28 mL g^{-1} (Mg-CUK-1). Scanning electron microscopy (SEM) and optical microscopy analyses of the as-synthesized materials without grinding revealed average crystallite sizes of 180 × 80, 15 × 15, and 180 × 50 μm for Co-CUK-1, Ni-CUK-1, and Mg-CUK-1, respectively (Figure S3). Crystals of Co- and Mg-CUK-1 displayed distorted tetragonal-like morphology. Their sizes are significantly larger than that of Ni-CUK-1.

As the hydrothermal stability of a porous solid is a prerequisite for heat transfer applications using water as a working fluid, the M-CUK-1 materials were exposed to boiling water. Co-CUK-1 and Ni-CUK-1 were found to maintain their crystal structures after hydrothermal treatment in water at 150 °C after 3 days (Figures 1b and S4). In addition, the solids that had been subjected to this hydrothermal treatment maintained their water sorption properties upon isolation (Figure S5). Mg-CUK-1 was found to be less stable than the two 3d-metal analogues when exposed to harsh refluxing water conditions; however, it is equally resistant to degradation under the lower-temperature (ca. 70 °C) working conditions required for adsorption cooling and dehumidification applications over prolonged periods. Indeed, Figure 2 reveals the hydrolytic stability of Mg-CUK-1 under multiple cyclic conditions, as illustrated by the plots of the water adsorption at 30 °C with a 60% relative humidity (RH), and after water desorption at 70 °C and 8% RH. These results suggest that Mg-CUK-1 is kinetically stable under hydrothermal conditions at elevated temperatures, which is in line with the highly electrostatic character of the Mg(II)−carboxylate-O bonds. Yaghi and co-workers emphasized the difference in terms of thermodynamic and kinetic stabilities of water-adsorbent MOFs in the presence of water at elevated temperatures.[39] It is assumed that the kinetic stability of Mg-CUK-1 under hydrolytic conditions is

DOI: 10.1021/acsami.9b02605
ACS Appl. Mater. Interfaces 2019, 11, 25778−25789

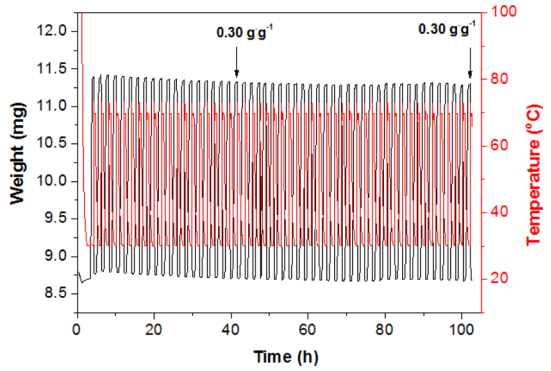

Figure 2. Hydrothermal stability of Mg-CUK-1 through TGA profile for 50 cycles of water adsorption−desorption. Test conditions: adsorption at 30 °C in humid nitrogen (60% RH) and desorption at 70 °C in N_2 gas with low humidity (8% RH). In both conditions the absolute humidity is the same (~0.016 kg H_2O/kg dry air). Prior to the multiple cycle experiment, the first cycle was carried out by a different condition such that Mg-CUK-1 is dehydrated at 150 °C for 1 h in dry N_2, hydrated at 30 °C in humid nitrogen (35% RH), and then dehydrated again at 70 °C in N_2 with low humidity (8% RH).

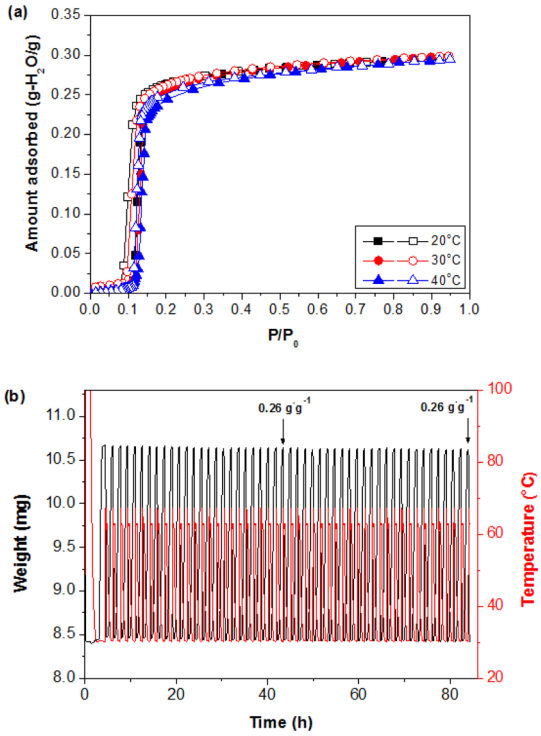

Figure 3. (a) Water sorption isotherms of Co-CUK-1 as a function of sorption temperatures (solid symbols: adsorption; open symbols: desorption); (b) TGA profile for 50 cycles of water adsorption−desorption of Co-CUK-1. Test conditions: adsorption at 30 °C in humid N_2 gas (35% RH) and desorption at 63 °C under N_2 with low humidity (6% RH). Absolute humidity in both cases is ~0.009 kg H_2O/kg dry air. Prior to the multiple cycle experiment, the first cycle was carried out by a different condition such that Co-CUK-1 is dehydrated at 150 °C for 1 h in dry N_2, hydrated at 30 °C in humid N_2 (35% RH), and then dehydrated again at 63 °C in nitrogen with low humidity (6% RH). In the upper graph, solid symbols and open symbols denote adsorption and desorption, respectively.

ascribed to the rigidity of its building node with high connectivity through triple bridging of Mg cations with two carboxylate bridges and a single-atom oxygen bridge.

2.2. Water Sorption Properties of Co-CUK-1. Water sorption isotherms for Co-CUK-1 measured at three different temperatures are depicted in Figure 3a. The water sorption isotherms show a sigmoidal shape with a very steep adsorption step of ca. $P/P_0 \approx 0.12$ (P_0 = saturation vapor pressure), indicating the presence of a uniform micropore. Most of the water uptake occurs at $P/P_0 < 0.25$. Considering a calculated crystal density of 1.46 g mL^{-1}, Co-CUK-1 exhibits a fairly high equilibrium water uptake of 0.28 g g^{-1} (equivalent to 0.41 mL mL^{-1}) at 30 °C and $P/P_0 = 0.4$. The adsorption−desorption isotherms also portray fully reversible water sorption with only a small hysteresis, which is indicative of easy water cycling regeneration by the sample.

The isosteric heat of water adsorption for Co-CUK-1 was calculated by applying the Clausius−Clapeyron equation for the adsorption isotherms collected at different temperatures.[40] The resulting isosteric heat of water adsorption was found to be 46.9 kJ mol^{-1} up to 0.22 g g^{-1} water uptake, which is above the evaporation enthalpy of water (40.7 kJ mol^{-1}) (Supporting Information Figure S6). In order to check the reliability of this estimated heat of water adsorption, we also applied the virial equation[41] to thermodynamic calculations of the adsorption isotherms (Supporting Information Figure S21). It was confirmed that the isosteric heats of adsorption could be accurately reproduced using virial coefficient fitting.

To verify the low-temperature desorption as well as the cycling stability of Co-CUK-1 between adsorption and desorption steps under working conditions in a hypothetical adsorption chiller, water sorption cycling experiments were then repeated 50 times: (i) each adsorption step was performed at 30 °C and 35% RH in N_2 gas; (ii) the desorption leg proceeded at 63 °C in N_2 gas with a lower RH = 6% (Figure 3b). The highly reversible cyclability test data show a negligible difference in working capacity (0.26 ± 0.01 g g^{-1}) between consecutive cycles, indicating a very high cycling durability of Co-CUK-1. This result clearly highlights the energy-efficient water sorption properties of this MOF, which is suitable for facile dehydration below 70 °C.

2.3. Water Adsorption Mechanism in Co-CUK-1. A direct comparison of Figure 4a,b shows that the experimental adsorption isotherm for Co-CUK-1 was accurately reproduced by Grand Canonical Monte Carlo (GCMC) simulations for Co-CUK-1. In particular, the onset of the pore-filling at P/P_0 = 0.12 is extremely well captured, whereas the slight deviation between the experimental and predicted water uptake at saturation is most probably associated with extra-adsorption at the external surface of the materials. The hydrophobic behavior of the MOF at the initial stage of the adsorption is also confirmed by the simulated adsorption enthalpy below the evaporation enthalpy of water (i.e., below P/P_0 = 0.12; see Supporting Information Figure S7), which gave an enthalpy of adsorption in the range of 45−60 kJ mol^{-1} above P/P_0 = 0.12. This prediction is consistent with the experimental isosteric heat of adsorption discussed above (Figure S6). This observation validates the microscopic models employed to represent both MOF and water, as well as the force field parameters used to describe the interactions between Co-CUK-1 and H_2O. The water adsorption mechanism was further explored to shed light on the adsorption behavior of Co-CUK-1 at the microscopic scale. We observed that at low

DOI: 10.1021/acsami.9b02605
ACS Appl. Mater. Interfaces 2019, 11, 25778−25789

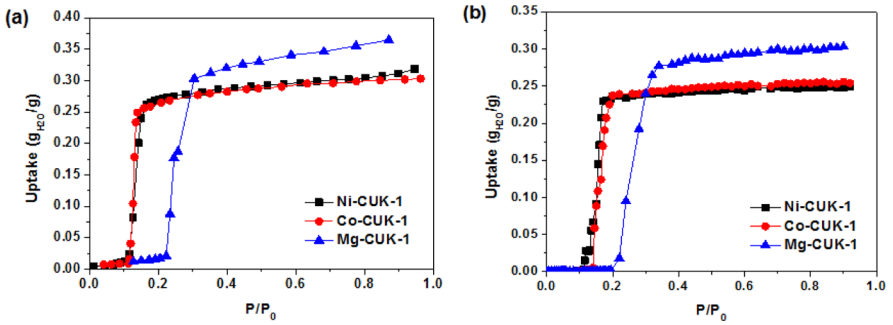

Figure 4. Comparison between the (a) experimental and the (b) GCMC-simulated water adsorption isotherms at 30 °C in Co-CUK-1, Ni-CUK-1, and Mg-CUK-1.

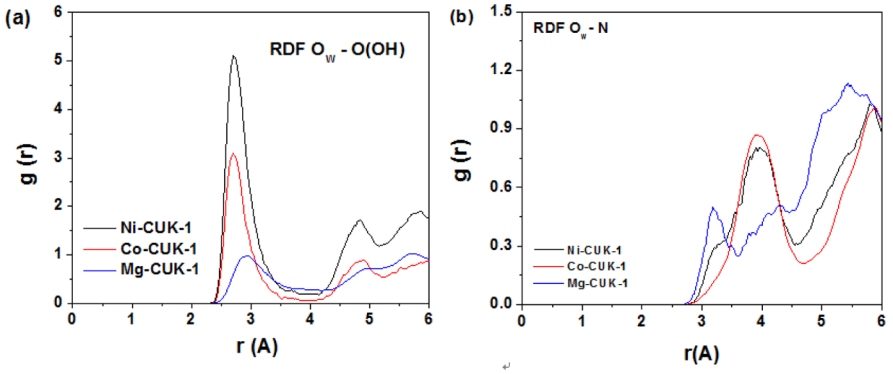

Figure 5. RDFs calculated at low coverage (one water molecule per simulation box) between the oxygen of the water molecules (O_W) and the (a) oxygen of the hydroxyl groups [O(OH)] and the (b) nitrogen (N) atoms of all CUK-1. These data are averaged over the MC snapshots collected at 30 °C.

coverage, the water molecules tend to interact preferentially with the hydroxyl groups (μ_3-OH) of the MOF framework.

As illustrated in Figure 5, there is a sharp peak in the radial distribution function (RDF) between the hydroxyl-O atoms and the oxygen of the water "W", with a mean O_W-O_{OH} distance of ca. 2.8 Å. This distance corresponds to the formation of a relatively strong hydrogen bond between the two species. This conclusion is also supported by the analysis of the density distributions for the water molecules, calculated at low coverage, which revealed that the guest molecules are preferentially located in the vicinity of the hydroxyl groups (Figure 5a). Once the water molecules interact with these hydrophilic centers, they trigger the clustering of further water molecules, forming an extensive network of water until the channel is fully filled (Supporting Information Figure S8).

The channel cross-sectional area (13.4 Å × 13.0 Å) in Co-CUK-1 is large enough to accommodate the formation of water clusters in cycles at saturation, which consist of between 4 and 7 molecules (see Supporting Information Figure S9) that share common edges or are linked through single water molecules. Such a predicted geometry is in good agreement with the pentameric drums that were found experimentally by SCXRD previously.[33]

2.4. Thermodynamic Performance of the Co-CUK-1/H_2O Working Pair. Evaluation of the achievable thermodynamic performance of adsorbent−water working pairs is crucial for the development of efficient adsorptive heat transformation systems (Figure S10). A full assessment and understanding of the ideal thermodynamic cycle between an adsorbent and water as an adsorbate is useful to choose working boundary conditions of adsorption chillers or heat pumps (Figure S11). This can be achieved experimentally through measurements of their main thermo-physical parameters, such as temperature (T), pressure (P), and water uptake (W).[8] Figure S12 illustrates a typical adsorption-driven thermodynamic cooling cycle for Co-CUK-1 based on water adsorption isobars collected at three saturated vapor pressures, P, which correspond to specific temperatures, that is, 5 °C (0.9 kPa), 10 °C (1.2 kPa), and 30 °C (4.2 kPa), respectively. The cycle consists of four steps: two for adsorption and two for desorption, in the order, isosteric cooling (D−C), isobaric adsorption (C−A), isosteric heating (A−B), and isobaric desorption (B−D).[8] During one such complete cycle, the adsorbed water as the working fluid ($W_{max} - W_{min}$), the working capacity, has taken up energy from the environment at a low temperature in the evaporator by its evaporation (Q_{evap}), while releasing heat in the adsorber at an intermediate temperature level upon adsorption. According to the cycle in Figure S12, an effective water uptake ($W_{max} - W_{min}$) for Co-CUK-1 was found to be 0.24 g g^{-1} (corresponding to 0.35 mL mL^{-1}) under the boundary condition, 5 °C (T_{ev})/30 °C (T_{con})/70 °C (T_{des}). When the evaporation temperature is increased to 10 °C, the effective water uptake also increases to 0.26 g g^{-1} (corresponding to 0.38 mL mL^{-1}).

As summarized in Table S1, the effective volumetric water uptake (0.35 mL mL^{-1}) of Co-CUK-1 at T_{ev} = 5 °C, T_{con} = 30 °C, and T_{des} = 70 °C is higher than that of benchmark adsorbents such as SAPO-34 (0.16 mL mL^{-1}), MIL-160 (0.12 mL mL^{-1}), and CAU-10-H (0.32 mL mL^{-1}). Clearly, Co-CUK-1 is therefore highly attractive as a water sorption medium and the discovery of these benchmark values encouraged us to further evaluate Co-CUK-1 for adsorptive

DOI: 10.1021/acsami.9b02605
ACS Appl. Mater. Interfaces 2019, 11, 25778−25789

chiller/heat pump applications under low driving temperatures. The choice of a driving temperature of 80 °C to regenerate the water-loaded adsorbent is directly in line with what is required for solar cooling applications, as this level of temperature can be achieved by the use of standard flat-plate solar heat collectors.[11] Similarly, a slightly lower driving temperature of 70 °C enables the utilization of waste heat emitted from a co-generation plant.[42] Kapteijn and co-workers have proposed standard conditions depending on the sorption temperature, water vapor pressure, and the evaporator and condenser temperatures in order to screen performances of water adsorbents envisaged for actual water adsorption chillers.[8] For thermodynamic calculations of water sorption performances,[8] we next considered two practical applications of M-CUK-1 for cooling and heat pump uses. First, it is useful to determine the thermodynamic efficiency, for which the coefficients of performance (COP_C or COP_H) for cooling or heat pump applications can be obtained, as a standard indicator to make a direct comparison of performances with SAPO-34 and other MOFs (including MIL-160,[9] CAU-10-H,[25] and MIP-200[30]). Two commonly used benchmark MOFs, MIL-100(Fe) and Al fumarate, each exhibit low adsorption at the evaporation temperature of 5 °C and hence their chilling performances are rather poor.[8] At an evaporation temperature of 10 °C their performances are improved; however, they remain much lower than that observed for the CUK-1 samples. Therefore, these materials were not considered further in the COP comparisons described below.

The COP_C for cooling is defined as the useful energy output (Q_{evap}) that is withdrawn by the evaporator, divided by the energy required as an input (Q_{des}) to desorb water from the adsorbent (also known as regeneration).[8] The alternative metric, COP_H, is applied to assess a material's performance in heat pump applications and it is defined as the summation of the useful energy output of Q_{evap} and Q_{ads} during the adsorption phase, divided by the energy input required for adsorbent regeneration (Q_{regen}).[8] Note that by convention, the energy output is given as a negative value as energy is released from the adsorption cycle, whereas the energy needed to effect regeneration is a positive quantity.

The calculated COP graphs for chiller and heat pump applications depending on evaporator and condenser temperatures are given in Figures 6 and 7. The cooling efficiency, COP_C, of Co-CUK-1 is 0.83 at T_{evap} = 5 °C, T_{con} = 30 °C, and T_{des} = 70 °C (Figure 6). The efficiency is distinctively higher than that of benchmark porous solids at low driving temperatures between 70 and 100 °C.

The COP_C for Co-CUK-1 remains higher than other adsorbents even when T_{evap} is increased from 5 to 10 and 15 °C without changing T_{con}. This behavior is in good agreement with the results of gravimetric and volumetric heat transferred from the evaporator in one cooling cycle as a function of the temperature lift at T_{des} = 70 °C, as well as the storable energy capacity as a function of T_{des} when T_{evap} = 10 °C and T_{con} = 30 °C (Table S1).

In addition to its cooling properties, Co-CUK-1 shows a very high thermal efficiency on heating at T_{evap} = 15 °C, T_{con} = 45 °C, and T_{des} = 85−100 °C (Figure 7). These values confirm that Co-CUK-1 outperforms other MOFs as well as SAPO-34 for heat pump applications. As far as we are aware, Co-CUK-1 is one of the best MOFs reported so far in terms of both cooling and heating efficiencies for potential chiller and heat pump applications. The small-pore alumino-phosphate AlPO-

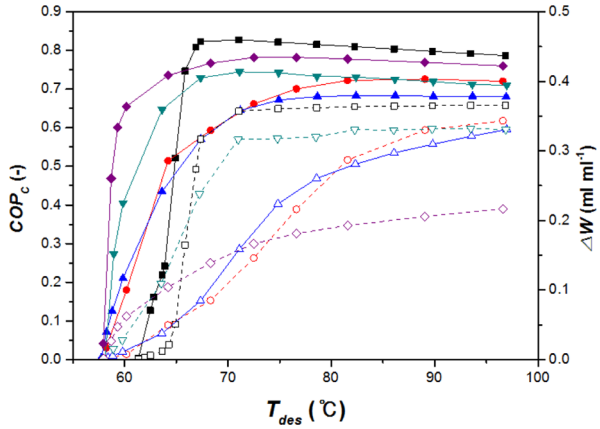

Figure 6. COP_C plots for chiller conditions (T_{ev} = 5 °C, T_{ads} = 30 °C) as a function of desorption temperature, T_{des} (closed symbols and full lines, left *y*-axis) and working capacity as volume of liquid water per volume of dry adsorbent, ΔW, as function of desorption temperature (open symbols, dashed lines, right *y*-axis) for Co-CUK-1 (black square), MIL-160 (red circle),[9] SAPO-34 (blue triangle),[8,9] CAU-10-H (green nabla),[9] and MIP-200 (violet diamond).[30]

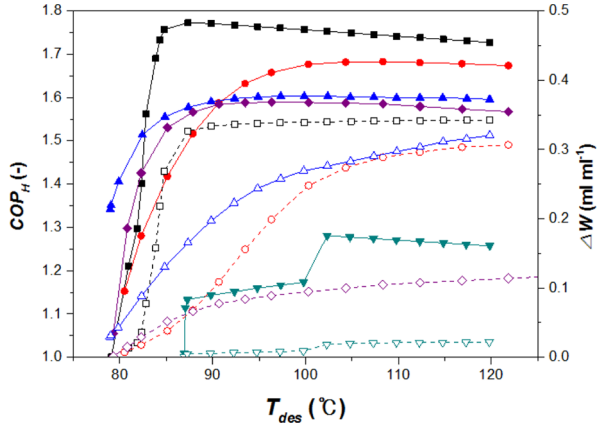

Figure 7. COP_H plots for heat pump conditions (T_{ev} = 15 °C, T_{ads} = 45 °C) as a function of desorption temperature, T_{des} (closed symbols and full lines, left *y*-axis) and working capacity as volume of liquid water per volume of dry adsorbent, ΔW, as function of desorption temperature (open symbols, dashed lines, right *y*-axis) for Co-CUK-1 (black square), MIL-160 (red circle),[9] SAPO-34 (blue triangle),[8,9] CAU-10-H (sky blue nabla),[9] and MIP-200 (violet diamond).[30]

LTA (or AlPO-42) has been also reported to be an excellent material for water sorption-based heat allocation and storage, superior to SAPO-34.[43] This material was confirmed to show high COP_C values above 70 °C,[30] but it was not selected as a comparable adsorbent in this work.

2.5. Effect of the Nature of the Framework Metal Ions (M^{2+}) on the Water Sorption Properties. Changing the metal ion in CUK-1 from Co to Ni or Mg was interestingly found to impact the water adsorption properties of M-CUK-1. As shown in Figure 4a, the adsorption isotherms for Co-CUK-1 and Ni-CUK-1 are similar, exhibiting a step-like shape with a pore filling at P/P_0 = 0.12; this is perhaps expected as both Co(II) and Ni(II) have very similar ionic radii and electronegativity.

However, the scenario differs more significantly for the 3s-metal-containing Mg-CUK-1, which shows a step in the experimental water adsorption isotherm at higher pressure (P/P_0 = 0.25) and a higher gravimetric uptake, because of the

DOI: 10.1021/acsami.9b02605
ACS Appl. Mater. Interfaces 2019, 11, 25778−25789

lower mass of Mg compared to Co or Ni. Meanwhile, the total number of water molecules adsorbed at saturation for all materials remains nearly the same at ca. 30 molecules per unit cell, indicating a similar volumetric capacity, and this is to be expected as the unit cell volumes are similar in all three materials. The higher hydrophobicity of Mg-CUK-1 compared to the two other analogues was also evidenced by GCMC calculations with the presence of the steep adsorption step at higher $P/P_0 \approx 0.2$ (Figure 4). One can see from Figure 5b that the RDF (O_W–O_{OH}) peak is of a significantly lower intensity for Mg-CUK-1 compared to the two other analogues. This is in line with a lower probability to find the water molecules interacting with the hydroxyl groups. This behavior can be explained by the analysis of the RDF between H_2O and the N atoms of the M-CUK-1 framework present in the organic node: Figure 5b clearly emphasizes that the water molecules tend to be located in the vicinity of these N atoms in the case of Mg-CUK-1, as shown by the presence of a well-defined peak at about 3.2 Å. This behavior is likely due to the significantly higher negative charge on the N atoms in Mg-CUK-1 versus those of the two 3d-metal analogues (see Table S2) which renders the organic node more attractive for the adsorbed water. This peculiarity of the Mg analogue is illustrated in Figure 8c, which clearly shows a significant distribution of

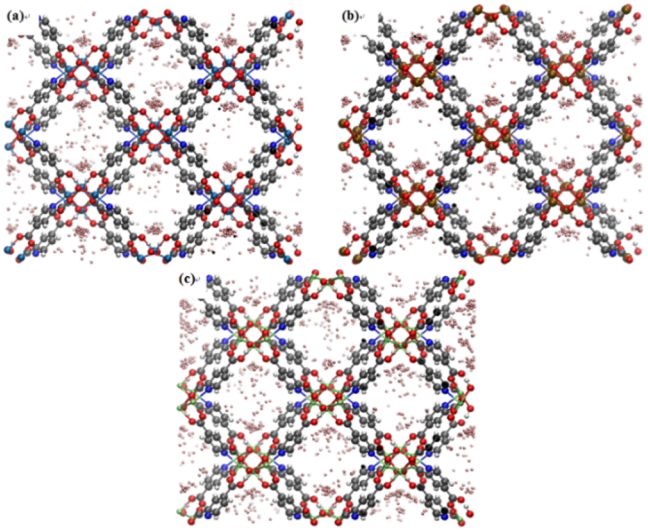

Figure 8. Center of mass distribution of water at low loading (one water molecule per simulation box) in the Ni-CUK-1 (a), Co-CUK-1 (b), and Mg-CUK-1 (c) averaged over the MC snapshots generated at 30 °C. Representation along the *a*-axis.

water in the region of the organic linker. Such a dual interaction between H_2O and the Mg-CUK-1 framework leads to a decrease of the overall affinity between the Mg-CUK-1 framework and water. This is confirmed by a lower water adsorption enthalpy calculated at very low coverage for this solid as compared to the two other analogues as can be seen in Figure S7. This trend holds true over the whole range of P/P_0. Interestingly, the water adsorption isotherm for Mg-CUK-1 at 40 °C clearly displays the two-step uptake (Figure S18), most probably assigned to the first coordination of water with the N atoms followed by a further pore filling with water.

The thermogravimetric weight-loss profiles of the three M-CUK-1 measured with a low ramping rate of heating (2 °C min^{-1}) reflects their energy-efficient character for water sorption (Figure S13). The weight loss profiles exhibit a single step of water removal below 70 °C, particularly 60 °C for Mg-CUK-1. In addition to this, water sorption cycling experiments were performed for Ni-CUK-1 and Mg-CUK-1 over 10 cycles (adsorption at 30 °C and 35% RH in N_2 gas; desorption at 55 °C and 10% RH in N_2 gas) (see Supporting Information Figures S14 and S15). These tests showed a negligible difference in weight loss (0.25 ± 0.01 g g^{-1} for Ni-CUK-1 and 0.29 ± 0.01 g g^{-1} for Mg-CUK-1) between cycles. It should be highlighted that these M-CUK-1 materials can be easily dehydrated at 55 °C.

To compare the relative water adsorption rates on the three M-CUK-1 analogues with SAPO-34, we collected their weight-gain profiles at the adsorption stage (30 °C and 35% RH) on the second cycle after water adsorption at 30 °C and 35% RH, followed by a regeneration at 63 °C and 10% RH in a nitrogen flow (100 mL min^{-1}). As shown in Figure S16, the relative adsorption rates of three M-CUK-1 could be competitive with that of the commercially water-adsorbent SAPO-34. However, precise kinetic analysis on water adsorption with M-CUK-1 is necessary for comparison. Table S1 compares the thermodynamic calculation results for the working capacities of water sorption, heat transferred from the evaporator, and energy storage capacities for the three M-CUK-1 and SAPO-34. In terms of cooling performances and energy storage capacities, all three M-CUK-1 materials clearly outperform SAPO-34. The performances for Co-CUK-1 and Ni-CUK-1 are very similar, whereas Mg-CUK-1 has moderately lower working capacities compared to the two other analogues, but conversely, this material has unique water sorption properties that result in a lower regeneration temperature (55 °C) because of its more hydrophobic character.

However, this MOF requires improving its hydrothermal stability because it showed 6.3 wt % loss of the initial working capacity during 30 cycles. In terms of COP_C and COP_H, the performances for Co-CUK-1 and Ni-CUK-1 are similar (Figures 9 and 10). In particular, Co-CUK-1 (1.77) and Ni-CUK-1 (1.84) have the highest COP values for heating among the MOFs reported so far. For Mg-CUK-1, there is a distinct advantage of incorporating Mg(II) ions into an adsorbent used at scale, as Mg(II) is a cheaper metal source than the

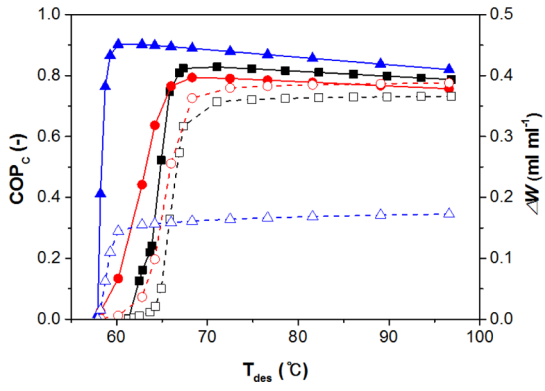

Figure 9. COP_C plots for chiller conditions (T_{ev} = 5 °C, T_{ads} = 30 °C) as a function of desorption temperature, T_{des} (closed symbols and full lines, left *y*-axis) and working capacity as volume of liquid water per volume of dry adsorbent, ΔW, as a function of desorption temperature (open symbols, dashed lines, right *y*-axis) for Co-CUK-1 (black square), Ni-CUK-1 (red circle), and Mg-CUK-1 (blue triangle).

DOI: 10.1021/acsami.9b02605
ACS Appl. Mater. Interfaces 2019, 11, 25778–25789

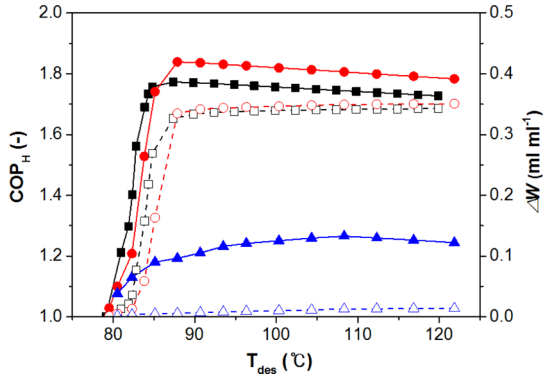

Figure 10. COP_H plots for heat pump conditions (T_{ev} = 15 °C, T_{ads} = 45 °C) as a function of desorption temperature, T_{des} (closed symbols and full lines, left *y*-axis) and working capacity as volume of liquid water per volume of dry adsorbent, ΔW, as a function of desorption temperature (open symbols, dashed lines, right *y*-axis) for Co-CUK-1 (black square), Ni-CUK-1 (red circle), and Mg-CUK-1 (blue triangle).

transition-metal ions Co or Ni, and Mg is also both nontoxic and biocompatible, which is preferential for many water sorption applications.

As shown in Figure 11 and Table S1, we estimated the gravimetric and volumetric heat values for the evaporative and

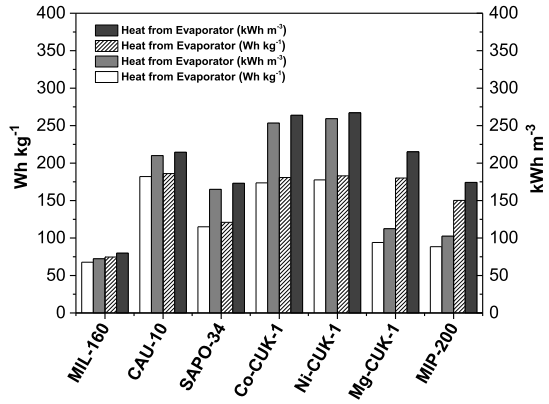

Figure 11. Gravimetric and volumetric heats from the evaporator calculated for M-CUK-1 and benchmark adsorbents. Boundary conditions: heats transferred from the evaporator in one cooling cycle at T_{ev} = 5 °C, T_{con} = 30 °C, and T_{des} = 70 °C (white and gray bars) and T_{ev} = 10 °C, T_{con} = 30 °C, and T_{des} = 70 °C (shaded and dark gray bars). White and shaded bars denote the gravimetric heats (W h kg^{-1}), whereas gray and dark gray bars indicate the volumetric heats (kW h m^{-3}).

heat storage capacities for the M-CUK-1 materials, as well as for some benchmark adsorbents under specific working conditions. Under a single cooling cycle (where T_{ev} = 5 °C (or 10 °C), T_{con} = 30 °C, and T_{des} = 70 °C), Ni- and Co-CUK-1 showed high volumetric heat values of evaporation and higher heat storage capacities compared with that for SAPO-34 and other MOFs, although the gravimetric heat capacities were slightly lower than the value previously reported for CAU-10. Mg-CUK-1 exhibited higher volumetric heat and heat storage capacity than those for SAPO-34 at evaporator temperatures of 10−20 °C. These results indicate that Mg-CUK-1 is advantageous at higher evaporator temperatures for adsorption cooling performance, whereas other CUK-1 materials are effective for low-temperature cooling below 10 °C. In contrast, MIP-200 was reported to be effective for adsorption cooling upon low-temperature regeneration (desorption, below 65 °C),[30] but the performance was reduced at higher regeneration temperatures (70 °C).

Considering the five requirements stated as key qualities for MOFs to act as efficient adsorbents, all three CUK-1 materials achieve high volumetric and gravimetric water sorption capacities; they display ideal step-type water adsorption−desorption isotherms with a high volumetric uptake of water between P/P_0 = 0.10−0.25; they enable facile regeneration at low driving temperatures (70 °C or lower); they display high thermal energy cooling efficiencies (for Ni- and Co-CUK-1) and heating (for Mg-CUK-1) and they were shown to be highly cyclable because of suitable levels of chemical and mechanical robustness. Therefore, it is evident that the water sorption properties of the CUK-1 materials outperform commercial water adsorbents including silica gel and SAPO-34, as well as several benchmark MOF adsorbents. Whereas MOFs can achieve unparalleled levels of water sorption performance, their synthesis costs and scalability in comparison to naturally occurring zeolitic sorbents continue to be a limiting step toward their implementation in large-scale platforms. Arguably, the CUK-1 materials lead the field in this regard because they are synthesized using simple reagents and water as the only solvent, and they can be prepared at scale using continuous microwave-assisted heating.

3. CONCLUSIONS

In comparison with other commercial benchmarks and existing MOFs that have been proposed for the chiller and/or heat pump applications, the three M-CUK-1 analogues described in this work displayed remarkable water sorption properties in terms of the five criteria required for advanced water adsorbents. In this study, thermodynamic calculations revealed that Co-CUK-1 and Ni-CUK-1 exhibit high efficiency for both chiller and heat pump applications considering low driving temperatures. In particular, Co-CUK-1 and Ni-CUK-1 had an excellent COP_H. Although Mg-CUK-1 presents a lower cooling performance compared to the two other analogues, this material displays excellent water sorption properties that permit easy regeneration at low temperature (55 °C), together with the use of environmentally benign, cheaper, and lighter Mg(II) ions in the framework. Mg-CUK-1 shows the best COP_C and a low desorption temperature although its working capacity is half that of the other CUK-1 materials. This work demonstrated that a joint experimental−computational approach combined with thermodynamic calculations is a powerful means to investigate the most important features of promising water adsorbents such as the M-CUK-1 materials. In particular, molecular simulations confirmed that this Mg-version showed a more pronounced hydrophobic character that makes this series of M-CUK-1 materials tunable, depending on the targeted applications and working conditions required.

4. EXPERIMENTAL SECTION

4.1. Typical Synthesis of CUK-1. *4.1.1. Synthesis of Co-CUK-1.* The hydrothermal synthesis of Co-CUK-1 from the reaction of the dianion of 2,4-pdcH_2 with hydrated $CoCl_2$ in a basic aqueous solution was performed at 200 °C for 15 h using a recipe already reported elsewhere.[31] After cooling, the crystalline solid was purified by brief (3 × 20 s) cycles of sonication in fresh H_2O (100 mL), followed by

DOI: 10.1021/acsami.9b02605
ACS Appl. Mater. Interfaces 2019, 11, 25778−25789

decanting of the cloudy supernatant. The solid was further treated with dimethylformamide or ethanol under stirring at 70 °C for 5 h. Then, large pink prismatic crystals were isolated (product yield: 67%).

4.1.2. Synthesis of Ni-CUK-1. A solution of pyridine-2,4-dicarboxylic acid (185 mg, 1.0 mmol) and KOH (1.0 M, 4.5 mL) was added to a stirred aqueous solution (3 mL) of nickel(II) chloride hexahydrate (357 mg, 1.5 mmol) to give a 3:2:9 ratio of Ni/L/OH.[32] The resulting solution was loaded in a 100 mL Teflon autoclave, which was heated to 200 °C for 15 h, and then cooled to room temperature. The bright green crystalline solid was purified by short cycles (3 × 60 s) of ultrasonic treatment in H_2O, and decanting off the cloudy supernatant. The solid was finally dried overnight at 100 °C (product yield: 65%).

4.1.3. Synthesis of Mg-CUK-1. 2,4-pdcH_2 (170 mg, 1.0 mmol) and KOH (2.0 M, 2.0 mL) in H_2O (2.0 cm^3) were added to a stirred solution of $Mg(NO_3)_2$-hydrate (380 mg, 1.5 mmol) in H_2O (3.0 mL) to give a viscous, opaque slurry, which was then transferred to a 100 mL Teflon-lined autoclave, heated at 210 °C for 15 h, and cooled for 6 h.[33] After cooling, the crystalline solid was purified by brief cycles of sonication in fresh H_2O (20 mL), followed by decantation of the cloudy supernatant to yield large, colorless prismatic crystals (product yield: 70%).

4.2. Characterization of CUK-1. PXRD patterns of CUK-1 were obtained using a Rigaku D/MAX IIIB diffractometer (operating at 2 kW) using Ni-filtered Cu Kα-radiation (40 kV, 30 mA, λ = 1.5406 Å) and a graphite crystal monochromator. The particle morphology and crystal size were analyzed by SEM (Philips, XL30S FEG). BET surface area measurements were performed using CO_2 adsorption–desorption isotherms at dry ice temperature (−78.5 °C) after dehydration under vacuum at 300 °C for 12 h using a Micromeritics Tristar 3020. Surface areas were evaluated using the BET method, and pore volume was taken by a single point method at P/P_0 = 0.99. TGA was carried out in a thermogravimetric analyzer (DT Q600, TA Instruments, Universal V4.5A). Analysis was performed in a dry air flow of 100 mL min^{-1}. The temperature was increased from 25 to 700 °C with a heating rate of 2 or 5 °C min^{-1}. Before each TGA measurement, samples were hydrated in a chamber with 70% RH at 30 °C for 2 days.

4.3. Water Sorption Measurements. Water sorption isotherms and test for adsorptive chiller have been measured by an intelligent gravimetric analyzer (IGA, Hiden Analytical Ltd.). The IGA was automatically operated to precisely control the water vapor pressure (1–95% RH) and temperature (20–100 °C). Prior to adsorption experiments, samples were dehydrated at 100 °C for 1 h under high vacuum (<10^{-6} Torr). Multiple cycles of water adsorption–desorption were performed using a thermogravimetric analyzer (TGA, DT Q600, TA Instruments, Universal V4.5A) connected with a humidity generator. The humidity was controlled by using two mass flow controllers and a humidified nitrogen gas flow was passed through a thermogravimetric balance. The adsorption profiles were measured at 30 °C in humid nitrogen with RH = 35%, whereas desorption data were collected between 55 and 70 °C in dry nitrogen (6–10% RH) with a cycle time of 3 h.

4.4. Molecular Simulations. GCMC simulations were carried out at 30 °C to predict the adsorption behavior of water in the different M-CUK-1 analogues using the Complex Adsorption and Diffusion Simulation Suite (CADSS) code. The simulation box was made of 12 conventional unit cells (3 × 2 × 2) maintaining the atoms fixed in their initial positions. A mixed set of universal force field[44] and DREIDING[45] force field parameters were adopted to describe the Lennard-Jones (LJ) parameters for the atoms in the inorganic and organic part of the MOF framework, whereas the partial charges carried by these atoms were derived at the density functional theory level (see Supporting Information). Water molecules were described by the TIP4P/2005 potential model.[36] The LJ contributions from the H-atoms of hydroxyl groups in the inorganic nodes were ignored in accordance with the strategy we validated in a previous study.[9] Further description of the derivation of the atomic partial charges and LJ parameters are given in the Supporting Information. The water/M-CUK-1 interactions considered the sum a coulombic term and a van der Waals contribution with the use of 12-6 LJ expression with parameters calculated using the Lorentz Berthelot equation. Whereas the long-range electrostatic interactions were handled using the Ewald summation technique, the van der Waals term was calculated using a cut-off distance of 12 Å. For each point in the adsorption isotherm, 2 × 10^8 Monte Carlo steps were used for both equilibration and production runs. The adsorption enthalpy at low coverage (ΔH) was calculated through configurational-bias Monte Carlo simulations performed in the *NVT* ensemble using the revised Widom's test particle insertion method. In order to gain insight into the configurational distributions of the adsorbed species in the different CUK-1, additional data were calculated at different fixed pressures (fixed number of water molecules) including the hydrogen bond networks and the RDFs of intermolecular atom-pairs.

4.5. Thermodynamic Calculations. The thermodynamic calculations of adsorption chiller and heat pump cycles are performed by an express method based on the methodology reported by De Lange et al.[8] The COP is adopted to illustrate the energy efficiency of a heat pump cycle from a thermodynamic perspective. The energy analysis allows the determination of the COP, which is a ratio of useful heating or cooling energy output provided to the work required. To be able to assess the COP of a working pair, knowledge of the enthalpy of adsorption is of prime importance.[8] As described in more detail in ref 8, isosteric heats of adsorption were estimated by the Clausius–Clapeyron equation and compensated by the virial equation.[46] The isosteric enthalpy of adsorption is calculated from isotherms at multiple temperatures by eq 1

$$\Delta_{ads}H_W = R\left(\frac{\partial \ln p}{\partial(1/T)}\right)_W \tag{1}$$

where $\Delta_{ads}H_W$ is the isosteric enthalpy of adsorption, R is the universal gas constant, p and T represent temperature and pressure, respectively, and W is the volume of water (liquid) adsorbed per volume of adsorbent (crystalline densities are used for the conversion).[8]

Furthermore, the virial equation was also used to calculate the steric heat of adsorption (Q_{st}) from isotherms measured at different temperatures.[46]

$$\ln p = \ln v + \left(\frac{1}{T}\right)\sum_{i=1}^{m} a_i v^{i-1} + \sum_{i=1}^{n} b_i v^{i-1} \tag{2}$$

where v is the amount adsorbed and a_i and b_i are empirical parameters.

The virial-type equation was applied compared with the Clausius–Clapeyron equation as shown in Figures S21–S27. A set of temperature-independent parameters a_i, which lead to direct evaluation of Q_{st} can be derived by fitting eq 2 continuously using adsorption isotherms obtained at different temperatures.

$$Q_{st} = -R\left(\frac{\partial \ln p}{\partial(1/T)}\right)_v = -R\sum_{i=1}^{m} a_i v^{i-1} \tag{3}$$

Using the two equations, it was confirmed that the isosteric enthalpies of adsorption for CUK-1 show overall a similar shape.

For calculation procedures, a characteristic curve needs to be constructed to transfer the loading from two dependent variables (p, T) to one, the adsorption potential, A, which is the molar Gibbs-free energy of adsorption with the opposite sign, defined as

$$A = RT \ln\left(\frac{p_o(T)}{p}\right) \tag{4}$$

where p_o is the temperature-dependent vapor pressure of the adsorbate of choice. The amount adsorbed should be expressed as volume occupied by the adsorbed phase. As the density of the adsorbed phase is often not known, the liquid phase density is used as approximation

DOI: 10.1021/acsami.9b02605
ACS Appl. Mater. Interfaces 2019, 11, 25778–25789

$$W = \frac{q(p, T)}{\rho_{liq}^{wf}(T)} \quad (5)$$

where q is the mass adsorbed, W is the volume liquid adsorbed, and ρ_{liq}^{wf} is the liquid density of the same adsorbate. If temperature invariance of W is assumed, all measured adsorption data should collapse onto one single "characteristic curve". An adsorption-driven heat pump cycle can be used for either heating or cooling. As the working pair (sorbent−sorbate) is known, only four distinct temperature levels need be defined to be able to determine the COP for either application.[8] Note that the desorption temperature is allowed to vary to investigate the required desorption temperature. The COP is defined as the useful energy output divided by the energy required as input. For heating, this becomes

$$COP_H = \frac{-(Q_{con} + Q_{ads})}{Q_{regen}} \quad (6)$$

where Q_{con} is the energy released during condensation and Q_{ads} is the energy released during adsorption. Both have a negative value as energy is withdrawn from the adsorption cycle. Q_{regen} is the energy required for regeneration of adsorbent. In this case, a positive quantity as energy is added to the system. For cooling, the coefficient of performance COP_C becomes

$$COP_C = \frac{Q_{ev}}{Q_{regen}} \quad (7)$$

where Q_{ev} is the energy withdrawn by the evaporator. Note that the COP_H should have a value between 1 and 2 and the COP_C is per definition not larger than unity. The specifics on how to exactly calculate these energetic contributions are explained in detail in ref 8. Please note, lastly, that the specific heat capacity is assumed to be 1 J g^{-1} K^{-1}, which is an average value for a variety of MOF materials. In fact, the actual value of this quantity has a negligible effect on the calculated COPs.

■ ASSOCIATED CONTENT

Supporting Information

The Supporting Information is available free of charge on the ACS Publications website at DOI: 10.1021/acsami.9b02605.

TGA profiles of fully hydrated CUK-1 samples under a dry N_2 flow;CO_2 adsorption isotherms of M-CUK-1 at −75°C; SEM and optical macroscopic images of as-synthesized Co-CUK-1, Ni-CUK-1, and Mg-CUK-1 samples; PXRD patterns of Ni-CUK-1 before and after hydrothermal treatment at 150°C for 3 days; TGA profiles of fully hydrated Co-CUK-1 and Ni-CUK-1 samples before and after hydrothermal treatment at 150°C for 3 days; isosteric enthalpy of adsorption for Co-CUK-1 and water as a function of loading and 95% confidence interval; water adsorption enthalpies computed for all CUK-1 frameworks as a function of the relative pressure at 30°C; comparison between simulated and experimental distribution of water at saturation in Mg-CUK-1; snapshot of arrangement of water molecules as interconnected rings as evidenced by GCMC simulations; illustration of a sorption-driven cooling system; thermodynamic cycle of an adsorption heat pump cycle; adsorption cooling thermodynamic cycle; relative TG weight-loss profiles, relative mass as a function of temperature of fully hydrated CUK-1 and SAPO-34 under a dry N_2 flow; thermogravimetric analysis profile for 10 cycles of water adsorption−desorption of Ni-CUK-1 and Mg-CUK-1; relative adsorption curves of CUK-1 and SAPO-34; identification of atom types in M-CUK-1; water adsorption isotherms of Ni-CUK-1 and Mg-CUK-1 at three adsorption temperatures; water sorption isotherms at 303 K for MIL-160 and MIP-200 and at 298 K for CAU-1-H and SAPO-34; illustration of calculation procedure on heat of adsorption by interpolation of MATLAB; water adsorption isotherm of Co-CUK-1 at 293 K fitted using the virial equation; isosteric enthalpy of adsorption for Co-CUK-1, Ni-CUK-1, and Mg-CUK-1 as a function of loading; characteristic curves of Co-CUK-1, Ni-CUK-1, and Mg-CUK-1 at different temperatures; coefficient of performance (COP_C) plots of Co-CUK-1 for chiller conditions; coefficient of performance (COP_H) for Co-CUK-1 for heat pump conditions; water sorption properties and energy storage capacities of water adsorbents; and atomic partial charges for each M-CUK-1 framework (PDF)

■ AUTHOR INFORMATION

Corresponding Authors

*E-mail: guillaume.maurin@univ-montp2.fr (G.M.).
*E-mail: smh@cm.utexas.edu (S.M.H.).
*E-mail: jschang@krict.re.kr (J.-S.C.).

ORCID

Hyungjun Kim: 0000-0001-8261-9381
Freek Kapteijn: 0000-0003-0575-7953
Simon M. Humphrey: 0000-0001-5379-4623
Jong-San Chang: 0000-0003-3640-8190

Author Contributions

J.S.L., J.W.Y., and P.G.M.M. contributed equally to this work.

Notes

The authors declare no competing financial interest.

■ ACKNOWLEDGMENTS

The Korean authors are grateful to the Global Frontier Center for Hybrid Interface Materials (GFHIM, grant no. NRF-2013M3A6B1078879) and the Center for Convergent Chemical Process (CCP, grant no. SKC1810-4) for financial support. Y. K. Hwang and U.-H. Lee (KRICT) are also acknowledged for their helpful discussions of the water sorption experiments. P.G.M.M. thanks the National Counsel of Technological and Scientific Development CNPQ for the scholarship; G.M. the Institut Universitaire de France for its support; S.M.H. acknowledges the Welch Foundation (F-1738) for financial support.

■ REFERENCES

(1) Anastas, P. T.; Kirchhoff, M. M. Origins, Current Status, and Future Challenges of Green Chemistry. *Acc. Chem. Res.* **2002**, *35*, 686−694.
(2) Sheldon, R. A. Green Solvents for Sustainable Organic Synthesis: State of the Art. *Green Chem.* **2005**, *7*, 267−278.
(3) Li, Q.; Piechna, J.; Müller, N. Design of a Novel Axial Impeller as a Part of Counter-rotating zxial compressor to compress water vapor as refrigerant. *Appl. Energy* **2011**, *88*, 3156−3168.
(4) Kilicarslan, A.; Müller, N. A Comparative Study of Water as a Refrigerant with Some Current Refrigerants. *Int. J. Energy Res.* **2005**, *29*, 947−959.
(5) Isaac, M.; van Vuuren, D. P. Modeling Global Residential Sector Energy Demand for Heating and Air Conditioning in the context of Climate Chage. *Energy Policy* **2009**, *37*, 507−521.
(6) Rogelj, J.; den Elzen, M.; Höhne, N.; Fransen, T.; Fekete, H.; Winkler, H.; Schaeffer, R.; Sha, F.; Riahi, K.; Meinshausen, M. Paris

Agreement climate proposals need a boost to keep warming well below 2 °C. *Nature* **2016**, *534*, 631−639.
(7) Ghafoor, A.; Munir, A. Worldwide Overview of Solar Thermal Cooling Technologies. *Renewable Sustainable Energy Rev.* **2015**, *43*, 763−774.
(8) De Lange, M. F.; Verouden, K. J. F. M.; Vlugt, T. J. H.; Gascon, J.; Kapteijn, F. Adsorption-Driven Heat Pumps: The Potential of Metal-Organic Frameworks. *Chem. Rev.* **2015**, *115*, 12205−12250.
(9) Cadiau, A.; Lee, J. S.; Damasceno Borges, D.; Fabry, P.; Devic, T.; Wharmby, M. T.; Martineau, C.; Foucher, D.; Taulelle, F.; Jun, C.-H.; Hwang, Y. K.; Stock, N.; De Lange, M. F.; Kapteijn, F.; Gascon, J.; Maurin, G.; Chang, J.-S.; Serre, C. Design of Hydrophilic Metal Organic Framework Water Adsorbents for Heat Reallocation. *Adv. Mater.* **2015**, *27*, 4775−4780.
(10) Wu, W.; Zhang, X.; Li, X.; Shi, W.; Wang, B. Comparisons of Different Working Pairs and Cycles on the Performance of Absorption Heat Pump for Heating and Domestic Hot Water in Cold Regions. *Appl. Therm. Eng.* **2012**, *48*, 349−358.
(11) Henninger, S. K.; Jeremias, F.; Kummer, H.; Schossig, P.; Henning, H.-M. Novel Sorption Materials for Solar Heating and Cooling. *Energy Procedia* **2012**, *30*, 279−288.
(12) Krajnc, A.; Varlec, J.; Mazaj, M.; Ristić, A.; Logar, N. Z.; Mali, G. Superior Performance of Microporous Alumino-phosphate with LTA Topology in Solar-Energy Storage and Heat Reallocation. *Adv. Energy Mater.* **2017**, *7*, 1601815.
(13) Freni, A.; Bonaccorsi, L.; Calabrese, L.; Caprì, A.; Frazzica, A.; Sapienza, A. SAPO-34 Coated Adsorbent Heat Exchanger for Adsorption Chillers. *Appl. Therm. Eng.* **2015**, *82*, 1−7.
(14) Burtch, N. C.; Jasuja, H.; Walton, K. S. Water Stability and Adsorption in Metal-Organic Frameworks. *Chem. Rev.* **2014**, *114*, 10575−10612.
(15) Küsgens, P.; Rose, M.; Senkovska, I.; Fröde, H.; Henschel, A.; Siegle, S.; Kaskel, S. Characterization of Metal-Organic Frameworks by Water Adsorption. *Microporous Mesoporous Mater.* **2009**, *120*, 325−330.
(16) Demir, H.; Mobedi, M.; Ülkü, S. A Review on Adsorption Heat Pump : Problems and Solutions. *Renewable Sustainable Energy Rev.* **2008**, *12*, 2381−2403.
(17) Kakiuchi, H.; Shimooka, S.; Iwade, M.; Oshima, K.; Yamazaki, M.; Terada, S.; Watanabe, H.; Takewaki, T.; Takewaki, T. Novel Water Vapor Adsorbent FAM-ZO1 and Its Applicability to and adsorption Heat Pump. *J. Chem. Eng. Jpn.* **2005**, *31*, 361−364.
(18) Sapienza, A.; Santamaria, S.; Frazzica, A.; Freni, A. Influence of The Management Strategy and Operating Conditions on the Performance of and Adsorption Chiller. *Energy* **2011**, *36*, 5532−5538.
(19) Zhou, H.-C.; Long, J. R.; Yaghi, O. M. Introduction to Metal-Organic Frameworks. *Chem. Rev.* **2012**, *112*, 673−674.
(20) Furukawa, S.; Reboul, J.; Diring, S.; Sumida, K.; Kitagawa, S. Structuring of Metal-Organic Frameworks at the Mesoscopic/Microscopic Scale. *Chem. Soc. Rev.* **2014**, *43*, 5700−5734.
(21) Maurin, G.; Serre, C.; Cooper, A.; Férey, G. The New Age of MOFs and of Their Porous-Related Solids. *Chem. Soc. Rev.* **2017**, *46*, 3104−3107.
(22) Chang, J.-S.; Hwang, Y. K.; Jhung, S. H.; Hong, D.-Y.; Seo, Y.-K. (KRICT). U.S. Patent 8,168,813 B2, 2012; Korea Patent 10-0803964 B1, 2008.
(23) Seo, Y.-K.; Yoon, J. W.; Lee, J. S.; Hwang, Y. K.; Jun, C.-H.; Chang, J.-S.; Wuttke, S.; Bazin, P.; Vimont, A.; Daturi, M.; Bourrelly, S.; Llewellyn, P. L.; Horcajada, P.; Serre, C.; Férey, G. Energy-Efficient Dehumidification Over Hierachically Porous Metal-Organic Frameworks as Advanced Water Adsorbents. *Adv. Mater.* **2012**, *24*, 806−810.
(24) Henninger, S. K.; Habib, H. A.; Janiak, C. MOFs as Adsorbents for Low Temperature Heating and Cooling Applications. *J. Am. Chem. Soc.* **2009**, *131*, 2776−2777.
(25) Lenzen, D.; Bendix, P.; Reinsch, H.; Fröhlich, D.; Kummer, H.; Möllers, M.; Hügenell, P. P. C.; Gläser, R.; Henninger, S.; Stock, N. Scalable Green Synthesis and Full-Scale Test of the Metal-Organic Framework CAU-10-H for Use in Adsorption-Driven Chillers. *Adv. Mater.* **2018**, *30*, 1705869.
(26) Kim, H.; Yang, S.; Rao, S. R.; Narayanan, S.; Kapustin, E. A.; Furukawa, H.; Umans, A. S.; Yaghi, O. M.; Wang, E. N. Water Harvesting form Air with Metal-Organic Frameworks Powered by Natural Sunlight. *Science* **2017**, *356*, 430−434.
(27) Abtab, S. M. T.; Alezi, D.; Bhatt, P. M.; Shkurenko, A.; Belmabkhout, Y.; Aggarwal, H.; Weselinski, L. J.; Alsadun, N.; Samin, U.; Hedhili, M. N.; Eddaoudi, M. Reticular Chemistry in Action: A Hydrolytically Stable MOF Capturing Twice Its Weight in Adsorbed Water. *Chem* **2018**, *4*, 94.
(28) Rieth, A. J.; Yang, S.; Wang, E. N.; Dincă, M. Record Atmospheric Fresh Water Capture and Heat Transfer with a Material Operating at the Water Uptake Reversibility Limit. *ACS Cent. Sci.* **2017**, *3*, 668−672.
(29) Kummer, H.; Jeremias, F.; Warlo, A.; Füldner, G.; Fröhlich, D.; Janiak, C.; Gläser, R.; Henninger, S. K. A Functional Full-Sacle Heat Exchanger Coated with Aluminum Fumarate Metal-Organic Framework for Adsorption Heat Transformation. *Ind. Eng. Chem. Res.* **2017**, *56*, 8393−8398.
(30) Wang, S.; Lee, J. S.; Wahiduzzaman, M.; Park, J.; Muschi, M.; Martineau-Corcos, C.; Tissot, A.; Cho, K. H.; Marrot, J.; Shepard, W.; Maurin, G.; Chang, J.-S.; Serre, C. A Robust Large-Pore Zirconium Carboxylate Metal-Organic Framework for Energy-Efficient Water-Sorption-Driven Refrigeration. *Nat. Energy* **2018**, *3*, 985−993.
(31) Humphrey, S. M.; Chang, J.-S.; Jhung, S. H.; Yoon, J. W.; Wood, P. T. Porous Cobalt(II)-Organic Frameworks with Corrugated Walls: Structurally Robust Gas-Sorption Materials. *Angew. Chem., Int. Ed.* **2007**, *46*, 272−275.
(32) Humphrey, S. M.; Weldon, G. F.; Wood, P. T. Pyridine-2,4-Dicarboxylate: A Versatile Building Block for the Preparation of Functional Coordination Polymers. *J. Nanosci. Nanotechnol.* **2010**, *10*, 34−48.
(33) Saccoccia, B.; Bohnsack, A. M.; Waggoner, N. W.; Cho, K. H.; Lee, J. S.; Hong, D.-Y.; Lynch, V. M.; Chang, J.-S.; Humphrey, S. M. Separation of p-Divinyl benzene by Selective Romm-Temperature Adsorption Inside Mg-CUK-1 Prepared by Aqueous Microwave Synthesis. *Angew. Chem., Int. Ed.* **2015**, *54*, 5394−5398.
(34) Humphrey, S. M.; Mole, R. A.; McPartlin, M.; McInnes, E. J. L.; Wood, P. T. Isolated Magnetic Clusters of Co(II) and Ni(II) within 3-Dimensional Organic Frameworks of 6-Mercaptonicotinic Acid: Unique Structural Topologies Based on Selectivity for Hard and Soft Coordination Environments. *Inorg. Chem.* **2005**, *44*, 5981−5983.
(35) Lin, R.-B.; Li, L.; Zhou, H.-L.; Wu, H.; He, C.; Li, S.; Krishna, R.; Li, J.; Zhou, W.; Chen, B. Molecular sieving of ethylene from ethane using a rigid metal-organic framework. *Nat. Mater.* **2018**, *17*, 1128−1133.
(36) Yoon, J. W.; Jhung, S. H.; Hwang, Y. K.; Humphrey, S. M.; Wood, P. T.; Chang, J.-S. Gas-Sorption Selectivity of CUK-1: A Porous Coordination Solid Made of Cobalt(II) and Pyridine-2,4-Dicarboxylic Acid. *Adv. Mater.* **2007**, *19*, 1830−1834.
(37) Yoon, J. W.; Lee, J. S.; Piburn, G. W.; Cho, K. H.; Jeon, K.; Lim, H.-K.; Kim, H.; Jun, C.-H.; Humphrey, S. M.; Krishna, R.; Chang, J.-S. Highly Selective Adsorption of p-Xylene over other C8 Aromatic Hydrocarbons by Co-CUK-1: A Combined Experimental and Theoretical Assessment. *Dalton Trans.* **2017**, *46*, 16096−16101.
(38) Fletcher, A. J.; Cussen, E. J.; Bradshaw, D.; Rosseinsky, M. J.; Thomas, K. M. Adsorption of Gases and Vapors on Nanoporous $Ni_2(4,4'\text{-Bipyridine})_3(NO_3)_4$ Metal-Organic Framework Materials Templated with Methanol and Ethanol: Structural Effects in Adsorption Kinetics. *J. Am. Chem. Soc.* **2004**, *126*, 9750−9759.
(39) Kalmutzki, M. J.; Diercks, C. S.; Yaghi, O. M. Metal-Organic Frameworks for Water Harvesting form Air. *Adv. Mater.* **2018**, *30*, 1704304.
(40) Freni, A.; Maggio, G.; Sapienza, A.; Frazzica, A.; Restuccia, G.; Vasta, S. Compatative Analysis of Promising Adsorbent/Adsrbate Pairs for Adsorptive Heat Pumping, Air Conditioning and Refrigeration. *Appl. Therm. Eng.* **2016**, *104*, 85−95.

DOI: 10.1021/acsami.9b02605
ACS Appl. Mater. Interfaces 2019, 11, 25778−25789

(41) Czepirski, L.; JagieŁŁo, J. Virial-Type Thermal Equation of Gas-Solid Adsorption. *Chem. Eng. Sci.* **1989**, *44*, 797−801.
(42) Enteria, N.; Yoshino, H.; Mochida, A. Review of the Advances in Open-Cycle Adsorption Air-conditioning Systems. *Renewable Sustainable Energy Rev.* **2013**, *28*, 265−289.
(43) Krajnc, A.; Varlec, J.; Mazaj, M.; Ristić, A.; Logar, N. Z.; Mali, G. Superior Performance of Microporous Aluminophos-phate with LTA Topology in Solar-Energy Storage and Heat Reallocation. *Adv. Energy Mater.* **2017**, *7*, 1601815.
(44) Rappe, A. K.; Casewit, C. J.; Colwell, K. S.; Goddard, W. A.; Skiff, W. M. UFF. A Full Periodic Table Force Field for Molecular Mechanics and Molecular Dynamics Simulations. *J. Am. Chem. Soc.* **1992**, *114*, 10024−10035.
(45) Mayo, S. L.; Olafson, B. D.; Goddard, W. A.; Goddard, I. DREIDING: A Generic Force Field for Molecular Simulations. *J. Phys. Chem.* **1990**, *94*, 8897−8909.
(46) Bandosz, T. J.; Jagiełło, J.; Schwarz, J. A. Adsorption of Sulfur Hexafluoride and Propane at Temperatures near Ambient on Pillared Clays. *J. Chem. Eng. Data* **1996**, *41*, 880−884.

DOI: 10.1021/acsami.9b02605
ACS Appl. Mater. Interfaces 2019, 11, 25778−25789